JACS
JOURNAL OF THE AMERICAN CHEMICAL SOCIETY

COMMUNICATION

pubs.acs.org/JACS

Imaging Multiple Conductance States in an Alamethicin Pore

Lydia M. Harriss, Bríd Cronin, James R. Thompson, and Mark I. Wallace*

Department of Chemistry, University of Oxford, 12 Mansfield Road, Oxford OX1 3TA, U.K.

Supporting Information

ABSTRACT: Alamethicin is the archetypal antimicrobial pore-forming peptide. Although the peptide has long been known to form pores of characteristic conductances in lipid membranes, the precise nature of these pores is not known. Simultaneous calcium-flux imaging and single-channel recording in a droplet interface bilayer allowed us to directly attribute multiple conductance states to a single point diffusing in the bilayer.

Antimicrobial peptides (AMPs) are a vital component of the innate immune response of all multicellular organisms.[1] Many AMPs are thought to function by permeabilizing the microbial cell membrane, either by disrupting membrane integrity[2,3] or by forming conducting pores in the membrane.[4,5] AMPs often act as broad-spectrum antibiotics and exhibit lower susceptibility to bacterial resistance than conventional therapeutics, characteristics that are thought to be related to their general mode of action. As such, AMPs have significant potential in the development of new antimicrobial agents.[6,7]

The pore-forming α-helical peptide alamethicin is perhaps the best studied AMP, primarily due to its use as a model of voltage-gated ion-channel conduction.[8,9] Alamethicin is generally believed to form pores by inserting α-helical peptides perpendicular to the bilayer, where the hydrophilic faces of multiple peptides align to form a water-filled channel.[10] This "barrel-stave" model of alamethicin pore structure[11,12] is based on a number of experimental measurements, including X-ray and NMR structures of the monomer,[13] in-plane neutron scattering,[14] and the power dependence of pore conductance on monomer concentration.[8] The most compelling evidence for channel formation are the current steps observed in single-channel electrical recording (SCR) of alamethicin; the conductance states appear in bursts, starting and finishing from the lowest conductance state. Although this evidence supports the conclusion that alamethicin conduction must occur via discrete pores present in the membrane, none of these techniques provide direct evidence that this behavior is caused by a single alamethicin pore.

We recently developed a new method for the generation of artificial lipid bilayers, which involves contacting the monolayers formed on a nanoliter aqueous droplet and a hydrogel layer immersed in an oil/lipid solution to create a bilayer (Figure 1A).[15,16] This method enables single-molecule fluorescence imaging and SCR from the bilayer.[16,17] Ca^{2+} flux imaging is a widely used technique for the study of calcium permeant channels, including those present in oocyte membranes and heart cells.[18,19] In this work, we exploit the features of droplet interface bilayers (DIBs) to study alamethicin pore formation using a combination of Ca^{2+} flux imaging and SCR. We report direct observation of multiple conductance states arising from individual channels present in the lipid bilayer.

DIBs were formed following our previously described method.[15,17] Briefly, an aqueous droplet (100 nL, 0.5 μM alamethicin, 0.4 mM EDTA, 50 μM Fluo-8H, 700 mM KCl, 10 mM HEPES, pH 7) and agarose substrate (1.8% w/v agarose, 100 mM $CaCl_2$, 500 mM KCl, 10 mM HEPES, pH 7) were brought together in a lipid (5.2 mM POPE, 1.6 mM POPG, 3:1) and hexadecane mixture to form a lipid bilayer (Figure 1A). Ag/AgCl electrodes were inserted into the droplet and the agarose substrate (ground). The DIB system, electrodes, and the headstage for the patch clamp amplifier were all enclosed in a purpose-built Faraday cage. Electrical currents were measured using an Axopatch 200B patch clamp amplifier (Axon Instruments). Data were recorded using Windows Electrophysiology Disk Recorder (WinEDR, Strathclyde Institute of Pharmacy and Biomedical Science), which was used to apply a postacquisition 1 kHz low-pass filter. To verify that Ca^{2+} flux imaging did not significantly perturb the behavior of the peptide, the electrical activity of alamethicin under these conditions was characterized (Figure 2). Current−voltage characteristics from individual conductance levels displayed nearly ohmic behavior at negative potentials, comparable to that observed previously for alamethicin.[20] The application of large (∼150 mV) positive potentials resulted in the rapid appearance of many alamethicin pores and breakdown of the bilayer, again as previously observed.[21]

Single-channel conductances from alamethicin pores were similar to those reported previously, and no pores were observed in the absence of the peptide (Supporting Information).

Ca^{2+} flux through individual alamethicin pores was visualized using the Ca^{2+} chelating dye, Fluo-8H, imaged by total internal reflection fluorescence (TIRF) microscopy (Figure 1B). TIRF was achieved through an oil immersion objective (60× Plan Apo, NA 1.4) using an inverted microscope (TE-2000, Nikon Instruments) and a 473 nm laser (Shanghai Dream Lasers Technology Co.). The emitted fluorescence was directed through a dichroic mirror and 525/50 nm band-pass filter before being imaged on an emCCD (iXon+, Andor Technology, 128 × 128 pixels).

When alamethicin was present in the droplet and a negative potential was applied, individual stable, diffusing fluorescent spots were observed in the bilayer (Figure 1B,C). Generally, the intensity of fluorescence from individual conductance states was seen to vary linearly with the applied potential. Fluorescent signals due to Ca^{2+} flux were localized using a single-particle tracking algorithm developed for ImageJ[22] by the Computational Biophysics Lab at ETH Zurich.[23] Analysis of the mean-squared displacement

Received: May 10, 2011
Published: August 17, 2011

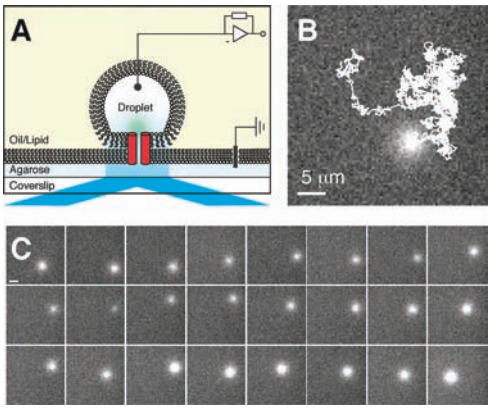

Figure 1. (A) Schematic of experiment. A bilayer was formed between an agarose substrate containing Ca^{2+} and an aqueous droplet containing alamethicin and Fluo-8H. Ion current through alamethicin (red cylinders) pores was detected on application of a potential difference using Ag/AgCl electrodes. Ca^{2+} ion flux was monitored fluorescently using TIRF microscopy. Multiple diffusing fluorescent spots were observed in the bilayer when alamethicin was present. (B) The diffusion trajectory of an example fluorescent spot is superimposed onto the initial image of the sequence. (C) Image sequence (10.6 ms/frame, sampled at 1 s intervals, 35.2 μm × 35.2 μm per component image) showing persistent fluorescent spots that exhibit distinct changes in intensity.

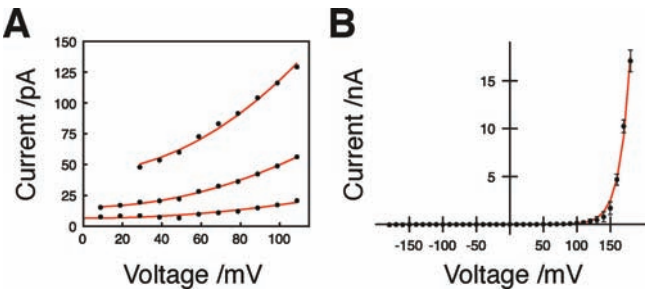

Figure 2. Electrical characterization of alamethicin in DHB. (A) Variation in the current levels of a single alamethicin pore over a range of voltages under the same conditions as those used for simultaneous electrical and Ca^{2+} flux imaging measurements. Mean current values for each level were obtained from a multipeak Gaussian fit to a histogram of the electrical recording. (Droplet: 0.5 μM alamethicin, 2 mM EDTA, and 50 μM Fluo-8H. Agarose substrate: 100 mM $CaCl_2$ and 500 mM KCl.) (B) In the absence of the components required for Ca^{2+} flux imaging, alamethicin also displayed macroscopic current−voltage characteristics consistent with previous reports. (Droplet: 0.5 μM alamethicin and 500 mM KCl. Agarose substrate: 500 mM KCl.) Data were fitted with an exponential function. Data points were averaged from five consecutive experiments on the same bilayer, and error bars show the standard deviation.

versus time for diffusion (Figure 1B) yields a diffusion coefficient of $1.4 \pm 0.3\,\mu m^2\,s^{-1}$, similar to that found using the fluorescence recovery after photobleaching of a fluorescently labeled alamethicin derivative.[24]

To enable extended observation of alamethicin pores, the substrate agarose concentration was increased (~2.5% w/v) to restrict pore mobility. The electrical behavior of the alamethicin was unchanged and still showed characteristic discrete conductance level behavior. Simultaneous measurement of the electrical conductance of the bilayer and Ca^{2+} flux imaging allowed

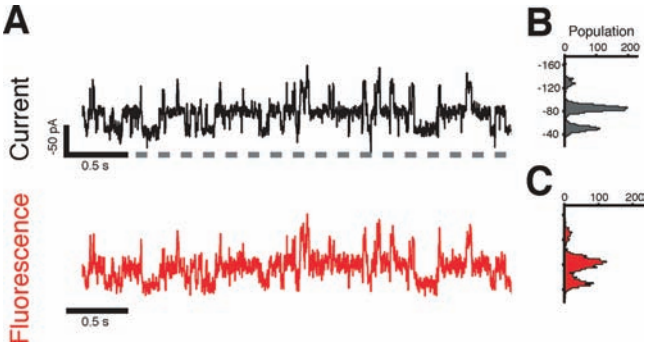

Figure 3. (A) Simultaneous SCR and Ca^{2+} flux of a single alamethicin pore exhibiting multiple conductance levels (conductances: 268 ± 39, 478 ± 43, and 744 ± 49 pS; 0.5 μM alamethicin). Current events corresponding to different conductance levels are clearly reflected in the fluorescence from a single alamethicin pore. The resolution of the electrical trace was decreased by linear interpolation to match the time resolution of the fluorescence measurement (2 ms exposure, 485.44 Hz). Histograms of the current (B) and fluorescence (C) data shown in (A) are also provided. Electrical and fluorescence data have been filtered using a step-preserving, running-average algorithm prior to binning. Details are given in the Supporting Information.

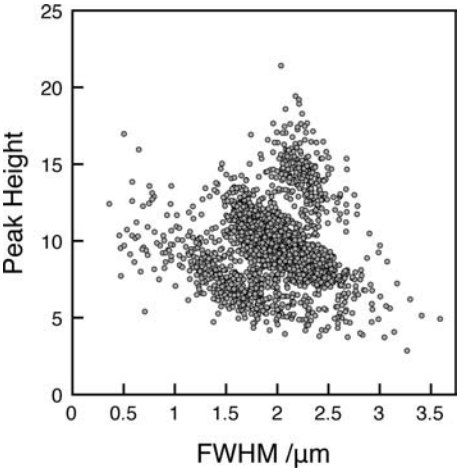

Figure 4. Dependence of spot peak height on spot width (fwhm) for the alamethicin pore in Figure 3 following 2D Gaussian fitting of the fluorescent spot. Each data point corresponds to a fit from a single frame. Three clusters of data points can be distinguished, corresponding to the three conductance levels observed.

observation of multiple conductance steps originating from a single alamethicin pore. Individual pores were observed to switch rapidly between distinct conductance states. For a bilayer containing a single pore, steps between discrete conductance states are correlated in the electrical and fluorescent measurements, confirming that multiple conductance states originate from a single pore (Figure 3).

We also examined the variation in fluorescence peak amplitude with full width at half-maximum (fwhm) from the 2D Gaussian fits of fluorescent spot intensity corresponding to an individual alamethicin pore (Figure 4). Three distinct bands can be seen, corresponding to the three distinct conductance states seen in Figure 3. The intensity threshold used to discriminate spots from background during our spot detection algorithm determines the minimum spot amplitude, and hence the absence

of data points at low amplitude. The optical diffraction limit determines the minimum fwhm. Figure 4 shows that, for each conductance state, the spot is well described by a Gaussian peak arising from a pore of essentially constant Ca^{2+} flux.

These experiments provide direct observation of the ion current through alamethicin pores on the bilayer and show that multiple conductance states do arise from punctate diffusing entities on the bilayer. Additionally, the variation in spot peak amplitude with fwhm places some limitations on the size of the ALM pore or pore complex. The smallest diffusing spots are at the Abbe diffraction limit (~400 nm in our instrument), which places a maximum size limit on the diffusing entities. Two possibilities are consistent with these observations: (1) Each diffusing spot is a single alamethicin pore with discrete conductance states. (2) Each spot is a number of alamethicin pores diffusing together as a collective unit. The size of such a collection must be smaller than the diffraction limit.

The observation of discrete diffusing punctate pores disfavors mechanisms of alamethicin action based on generalized disruption of membrane integrity. However, these experiments cannot distinguish between other models of pore action,[25,26] including the barrel-stave model and those that attribute pore gating to a conformational change of the peptide molecule.[13]

The primary limitation of the current work is that we do not determine the number of peptides contributing to a specific state, or whether there is a mechanism responsible for peptides' addition to or departure from the pore. A combination of single-molecule imaging and photobleaching step-counting[27] of fluorescently labeled alamethicin should reveal these details. We anticipate that similar ion-flux imaging experiments using droplet interface bilayers will prove to be a useful tool in studying other pore-forming antimicrobial peptides, both to understand membrane permeabilization mechanisms and to identify new antimicrobial agents.

■ ASSOCIATED CONTENT

Supporting Information. Detailed experimental methods and a video of diffusing pores. This material is available free of charge via the Internet at http://pubs.acs.org.

■ AUTHOR INFORMATION

Corresponding Author
mark.wallace@chem.ox.ac.uk

■ ACKNOWLEDGMENT

This work was supported by the BBSRC and the EPSRC. B.C. is an EPSRC Postdoctoral Research Fellow. L.M.H. was supported via a Life Science Interface Doctoral Training Centre Scholarship.

■ REFERENCES

(1) Zasloff, M. *Nature* **2002**, *415*, 389–395.
(2) Pouny, Y.; Rapaport, D.; Mor, A.; Nicolas, P.; Shai, Y. *Biochemistry* **1992**, *31*, 12416–12423.
(3) Gazit, E.; Miller, I. R.; Biggin, P. C.; Sansom, M. S.; Shai, Y. *J. Mol. Biol.* **1996**, *258*, 860–870.
(4) He, K.; Ludtke, S. J.; Huang, H. W.; Worcester, D. L. *Biochemistry* **1995**, *34*, 15614–15618.
(5) Leitgeb, B.; Szekeres, A.; Manczinger, L.; Vágvölgyi, C.; Kredics, L. *Chem. Biodivers.* **2007**, *4*, 1027–1051.
(6) Straus, S. K.; Hancock, R. E. *Biochim. Biophys. Acta* **2006**, *1758*, 1215–1223.
(7) Majd, S.; Yusko, E. C.; Billeh, Y. N.; Macrae, M. X.; Yang, J.; Mayer, M. *Curr. Opin. Biotechnol.* **2010**, *21*, 439–476.
(8) Hall, J. E.; Vodyanoy, I.; Balasubramanian, T. M.; Marshall, G. R. *Biophys. J.* **1984**, *45*, 233–247.
(9) Meyer, C. E.; Reusser, F. *Experientia* **1967**, *23*, 85–86.
(10) Sansom, M. S. P. *Q. Rev. Biophys.* **1993**, *26*, 365–421.
(11) Baumann, G.; Mueller, P. *J. Supramol. Struct.* **1974**, *2*, 538–557.
(12) Boheim, G. *J. Membr. Biol.* **1974**, *19*, 277–303.
(13) Fox, R. O.; Richards, F. M. *Nature* **1982**, *300*, 325–330.
(14) He, K.; Ludtke, S. J.; Heller, W. T.; Huang, H. W. *Biophys. J.* **1996**, *71*, 2669–2679.
(15) Bayley, H.; Cronin, B.; Heron, A.; Holden, M. A.; Hwang, W. L.; Syeda, R.; Thompson, J.; Wallace, M. *Mol. Biosyst.* **2008**, *4*, 1191–1208.
(16) Heron, A. J.; Thompson, J. R.; Cronin, B.; Bayley, H.; Wallace, M. I. *J. Am. Chem. Soc.* **2009**, *131*, 1652–1653.
(17) Thompson, J. R.; Heron, A. J.; Santoso, Y.; Wallace, M. I. *Nano Lett.* **2007**, *7*, 3875–3878.
(18) Smith, I. F.; Parker, I. *Proc. Natl. Acad. Sci. U.S.A.* **2009**, *106*, 6404–6409.
(19) Wang, S. Q.; Song, L. S.; Lakatta, E. G.; Cheng, H. *Nature* **2001**, *410*, 592–596.
(20) Eisenberg, M.; Hall, J. E.; Mead, C. A. *J. Membr. Biol.* **1973**, *14*, 143–176.
(21) Mueller, P.; Rudin, D. O. *Nature* **1968**, *217*, 713–719.
(22) Rasband, W. S. *ImageJ*; U.S. National Institutes of Health: Bethesda, MD, 1997−2011; http://imagej.nih.gov/ij/.
(23) Sbalzarini, I. F.; Koumoutsakos, P. *J. Struct. Biol.* **2005**, *151*, 182–195.
(24) Helluin, O.; Dugast, J. Y.; Molle, G.; Mackie, A. R.; Ladha, S.; Duclohier, H. *Biochim. Biophys. Acta* **1997**, *1330*, 284–292.
(25) Woolley, G. A.; Wallace, B. A. *J. Membr. Biol.* **1992**, *129*, 109–136.
(26) Latorre, R.; Alvarez, O. *Physiol. Rev.* **1981**, *61*, 77–150.
(27) Das, S. K.; Darshi, M.; Cheley, S.; Wallace, M. I.; Bayley, H. *Chembiochem* **2007**, *8*, 994–999.